Heat Dissipation of Transparent Graphene Defoggers

*Jung Jun Bae, Seong Chu Lim, Gang Hee Han, Young Woo Jo, Dinh Loc Doung, Eun Sung Kim, Seung Jin Chae, Ta Quang Huy, Nguyen Van Luan, and Young Hee Lee**

In spite of recent successful demonstrations of flexible and transparent graphene heaters, the underlying heat-transfer mechanism is not understood due to the complexity of the heating system. Here, graphene/glass defoggers are fabricated and the dynamic response of the temperature as a function of input electrical power is measured. The graphene/glass defoggers reveal shorter response times than Cr/glass defoggers. Furthermore, the saturated temperature of the graphene/glass defoggers is higher than for Cr/glass defoggers at a given input electrical power. The observed dynamic response to temperature is well-fitted to the power-balance model. The response time of graphene/glass defogger is shorter by 44% than that of the Cr/glass defogger. The convective heat-transfer coefficient of graphene is 12.4×10^{-4} W cm^{-2} °C^{-1}, similar to that of glass (11.1×10^{-4} W cm^{-2} °C^{-1}) but smaller than that of chromium (17.1×10^{-4} W cm^{-2} °C^{-1}). The graphene-based system reveals the lowest convective heat-transfer coefficient due to its ideal flat surface compared to its counterparts of carbon nanotubes (CNTs) and reduced graphene oxide (RGO)-based systems.

1. Introduction

Graphene, which is flexible,[1,2] highly transparent[3] and electrically conductive,[4,5] has unique potential for use as a flexible transparent heater. Yet the buoyant mass of a single graphene layer, in contrast to a conventional metal film, limits the substrate from being elevated to high temperature. Nevertheless, graphene can be utilized in various new functional devices, such as outdoor panel displays and vehicle front-window defrosters and defoggers. Recently, various nanostructured carbon materials, such as carbon nanotubes (CNTs),[6–10] reduced graphene oxide (RGO),[11] and graphene,[12] have been introduced for flexible transparent heaters. In particular, large-area graphene synthesis (for example, 40 in. diameter) and robust transfer processes are available,[13] which opens the possibility of developing flexible transparent heaters and defoggers for numerous functional devices.

J. J. Bae, Dr. S. C. Lim, Dr. G. H. Han, Y. W. Jo, D. L. Doung, E. S. Kim, S. J. Chae, T. Q. Huy, N. V. Luan, Prof. Y. H. Lee
BK21 Physics Division, Department of Energy Science, and Center for Nanotubes and Nanostructured Composites
Sungkyunkwan Advanced Institute of Nanotechnology
Sungkyunkwan University (SKKU)
Suwon 440-746, Korea
E-mail: leeyoung@skku.edu

DOI: 10.1002/adfm.201201155

Several previous reports on nanocarbon-based heaters describe the heat performance of the heater system using the maximum temperature attained for a given voltage and input power.[6–12] It has been reported that lowering the sheet resistance of nanocarbon-based film is the key factor in maximizing power performance. In thermally isolated systems, the temperature increase of the system is proportional to the input power, with the temperature increasing indefinitely as the input power supply is kept constant. In real systems, heat losses, including radiative and convective, from the surface of materials is inevitable, so that an equilibrium temperature if eventually reached due to heat balance.[14,15] Since nanocarbon-based heaters are limited to low temperature (less than around 100 °C) and thus are appropriate for use as defoggers, radiative heat loss can be negligible. Heat transfer takes places through two interfaces: i) conductive heat transfer through the solid(substrate)–solid (nanocarbon) interface, mediated by coupled phonons between two systems and ii) convective heat transfer at the solid–air interface, mediated by adsorbed ambient molecules via an adsorption/desorption process. Although conductive heat transfer through the solid (substrate)–solid (graphene) interface has been described,[16–22] there are no reports on convective heat loss at the solid–air interface in nanocarbon-based systems. While the former determines mainly the conductive heat-transfer rate, the latter determines mainly the final temperature of the defogger system. Therefore, the final temperature is strongly dependent on the convective heat loss, which is in general material-dependent.

The purpose of this paper is to investigate the effect of heat dissipation on the graphene/glass system, in particular its influence on the final temperature and its power dependence. We synthesized monolayer graphene on copper foil using thermal chemical vapor deposition (CVD) and transferred several layers of graphene onto glass substrate. The sheet resistance of the graphene layers was further reduced by the $AuCl_3$ layer-by-layer (LbL) doping technique.[23] Chromium metal film with equivalent sheet resistance to the prepared graphene heater was also prepared on the same glass substrate to elucidate the difference. By constructing a theoretical power-balance model, we were able to obtain physical parameter estimates of the heating rate constant, the convective heat-transfer coefficient, and the effective specific heat capacity of the heating system. We found that the final temperature is linearly proportional to the input power but

is not altered by the modified sheet resistance of the graphene film with doping for a given input power. Instead, the sheet resistance directly influences the limit of operation voltage, not the input power. The final temperature of the graphene/glass system was higher than that of the Cr/glass system due to a smaller convective heat-transfer coefficient. The convective heat-transfer mechanism was explained in terms of competition between direct scattering and trapping–desorption processes of ambient gases. Heat conduction at the solid–air interface was more efficient on the chromium surface than graphene surface, due to the larger adsorption energies of ambient gas molecules, such as O_2, N_2, and H_2O, on the chromium surface. By extracting the convective heat-transfer coefficients of carbon nanotubes (CNTs) and reduced graphene oxide (RGO)-based systems, we found that the graphene-based system revealed the lower coefficient, due to its ideal flat surface.

2. Results and Discussion

A graphene defogger consists of graphene transferred onto glass substrate and electrode formation on top of the graphene (**Figure 1**a). Input power is supplied to Cr/Au electrodes formed on top of the graphene defogger. Graphene is heated first by Joule heating, where heat is transferred to the glass substrate by conduction. Heat can be simultaneously dissipated through convection and radiation from both surfaces. Therefore, a steady-state will be formed eventually, with a final equilibrium temperature. CVD-grown large-area graphene on Cu foil is used for the graphene defogger. To transfer the graphene onto the glass substrate, PMMA is coated first on the graphene/Cu; the Cu foil is then etched away (Figure 1b). The resulting PMMA/graphene is placed on the glass substrate, followed by the removal of the PMMA. This process is repeated a few times to obtain a several-layer graphene defogger. Doping of $AuCl_3$ by solution dropping is done to improve sheet resistance.

Two samples of graphene were prepared: i) pristine trilayer (3L) graphene (2×2 cm^2) with a sheet resistance of 403 Ω sq^{-1} and a series resistance of 393 Ω with transmittance of approximately 92%, and, ii) $AuCl_3$-doped 3L graphene with a series resistance of 66 Ω and a transmittance of approximately 90%. **Figure 2**a shows the time evolution of temperature increase for a 3L graphene sample when the input power was supplied with a constant voltage. The temperature increased exponentially with time and reached a saturated equilibrium value at long time limit. The saturated temperature increased with the input power. Similar behaviors were observed for $AuCl_3$-doped 3L graphene sample, as shown in Figure 2b. One remarkable difference is the voltage required to reach the saturated temperature. Figure 2c shows the saturated temperature as a function of applied voltage for two samples. In order to obtain the same temperature, the doped sample requires less voltage than the pristine sample. For instance, to reach around 80 °C, the doped sample requires an input voltage of 10 V, smaller than the 24 V for the pristine sample. On the other hand, temperature dependence on the input electrical power was almost identical for two samples (Figure 2d). The inverse of the slope was 15.5×10^{-4} W cm^{-2} °C^{-1}, which is an area-dependent value. Our observations emphasize that improving sheet resistance does not increase the final temperature of the heating system for a given input power, but reduce the operation voltage.

To elucidate the difference between the graphene defogger and conventional metal thin-films, a chromium-deposited glass defogger with similar resistance (approximately 150 Ω) to the doped-3L graphene was used. Although the general trend of temperature changes seems to be similar (see the Supporting Information, Figure S1), the power dependence and the response time are slightly different, as shown in **Figure 3**a. It is also intriguing to note that the power dependence on the temperature reveals appreciable differences, viz., less power is required to obtain the same saturated temperature in the graphene/glass defogger (Figure 3b). Deviations from sample to sample (indicated by different symbols in Figure 3b) were not appreciable, validating our measurements. This implies that Cr thin film and graphene have different heat dissipation mechanisms.

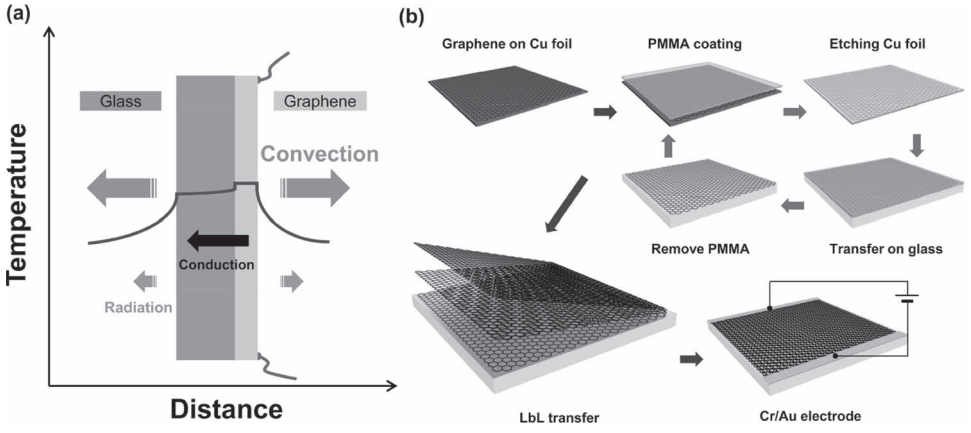

Figure 1. a) Schematic of heat transfer in a graphene defogger,showingsubstrates and expected temperature profile over the cross-section. b) LbL transfer process of graphene on to glass substrate.

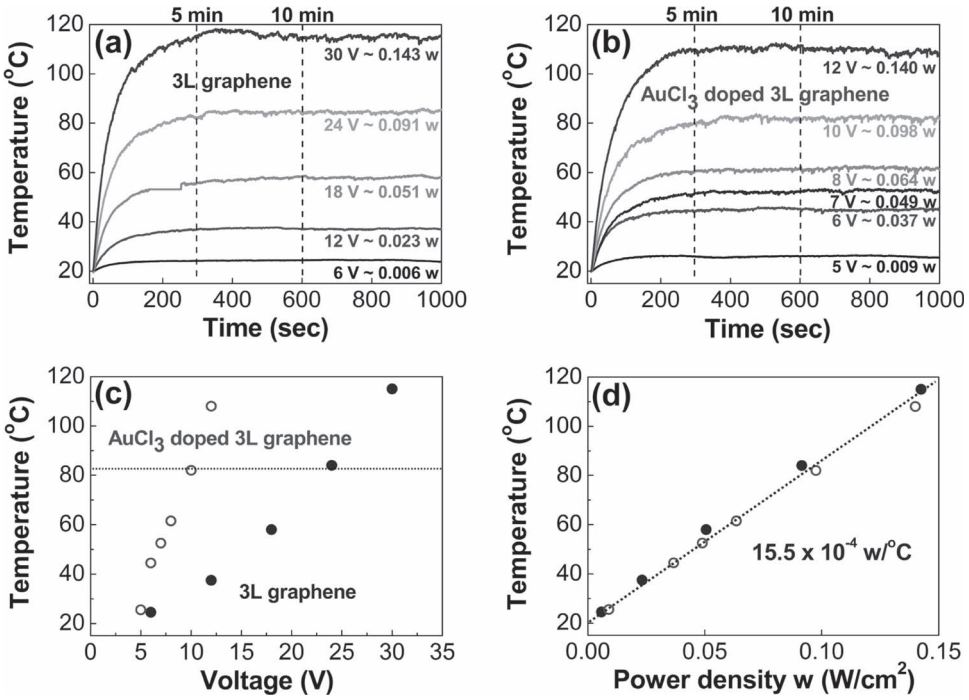

Figure 2. Temperature profiles of: a) 3L graphene defogger and b) $AuCl_3$-doped 3L graphene defogger at different input power densities. c) Saturated temperature as a function of input voltage. d) Saturated temperature as a function of input electrical power density. Area: glass substrate (4 cm × 4 cm), graphene (2 cm × 2 cm).

In general, the temperature of the heating system is balanced between input power and heat loss:

$$mc\frac{\mathrm{d}T(t)}{\mathrm{d}t} = VI - (Q_c - Q_r) \tag{1}$$

where m, c, T, and t are the mass ($m = m_{glass} + m_{graphene}$ or m_{Cr}), specific heat capacity, temperature of the heating system, and time, respectively; V and I are input voltage and current, respectively; and Q_c and Q_r are the convective power loss and radiative power loss, respectively. Here, the radiative heat power loss is expressed by the Stefan-Boltzmann law,

$$Q_r = \varepsilon\sigma A\left(T^4 - T_s^4\right) \tag{2}$$

where ε is the surface emissivity, σ the Stefan-Boltzmann constant (5.67×10^{-8} W m^{-2} °C^{-4}), A the surface area, and T_s the initial surface temperature. Convective heat power loss is expressed by,

$$Q_c = hA\left(T - T_s\right) \tag{3}$$

where h is the convective heat-transfer coefficient. At long time limit, where the temperature has no time dependence, the input power is balanced by the heat power loss. By presuming that radiative heat power loss is negligible compared to convective heat power loss, which will be shown later, we obtained the solution to Equation 1:

$$T - T_s = \Delta T\left(1 - e^{-t/\tau}\right) \tag{4}$$

where $\Delta T = VI/(hA)$ and $\tau = hA/(mc)$. It is obvious that the temperature change relies on the input power, convective heat-transfer coefficient, and the cross-sectional area. Simple doping

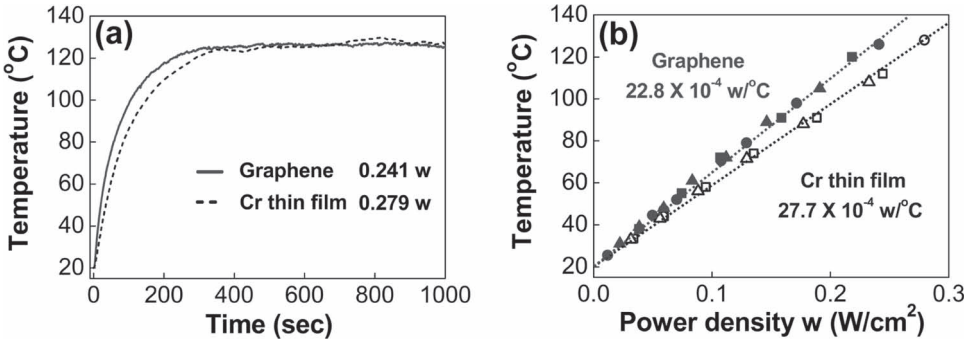

Figure 3. a) Temperature profile of two defoggers reaching the similar saturated temperature (different power density). b) Saturated temperature vs. electrical power density of graphene and Cr thin-film defoggers. Area: glass substrate (3.5 cm × 3.5 cm), graphene and Cr thin film (2.5 cm × 2.5 cm).

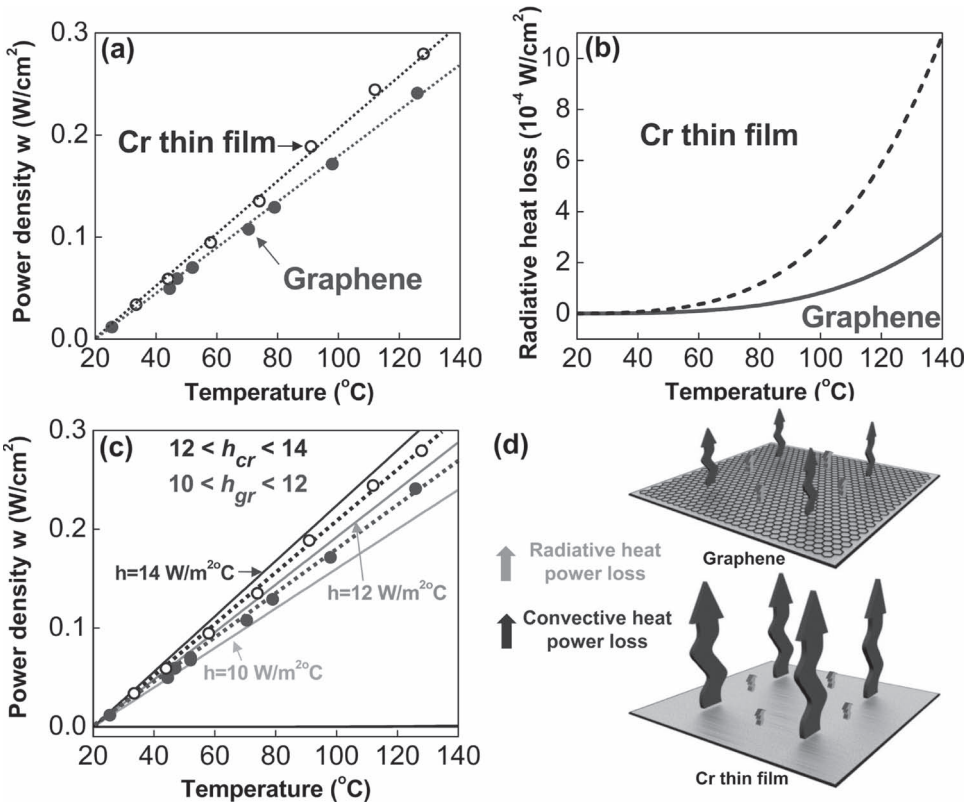

Figure 4. a) Electrical power density vs. saturated temperature of graphene/glass and Cr thin film/glass systems. b) Theoretical radiative heat power loss of two systems as a function of temperature ($\varepsilon_{Graphene} = 0.023$, $\varepsilon_{Cr} = 0.08$).[21,24,25] c) Convective heat power loss for various presumed convective heat-transfer coefficients with experimentally observed values for graphene (solid circles) and Cr thin-film (open circles) systems. d) Visualization of convective and radiative heat power loss for both systems.

of $AuCl_3$ on graphene, which involves charge transfer, does not alter the heat-transfer coefficient as observed in Figure 2. On the other hand, the Cr thin film shows a different saturated temperature to graphene for a given input power, as observed in Figure 3b.

To describe the input power dependence on the temperature in Equation 1, the input power vs. temperature was plotted again in **Figure 4**a. By using values of the material parameters, the radiative heat loss, based on Stefan-Boltzmann's law, was found and is plotted in Figure 4b. Graphene has much less radiative loss due to its lower emissivity. Yet, even in the high temperature region up to 140 °C, radiative heat loss is of the order of 10^{-4} W cm^{-2}, which is much less than the observed values in Figure 4a. Therefore radiative heat loss is negligible and our assumption used in solving Equation 1 is valid. The convective heat loss based on assumed values, of 10–14 W m^{-2} °C^{-1}, fits the observed curves (Figure 4a) well, as shown in Figure 4c. Therefore, the solution obtained in the current approach by ignoring radiative heat loss is valid. Since the saturated temperature change $\Delta T = VI/(hA)$, depends on the input power and convective heat-transfer coefficient, h can be obtained directly fitting the slope of Figure 4a; the resulting values are listed in **Table 1**. The convective heat-transfer coefficient of graphene/glass defogger is smaller than that of the Cr/glass defogger, which is expected from the lower power consumption of the graphene defogger. By fitting Equation 4 to the experimental curves as shown in Figure 3a, the time constant τ was obtained, listed in Table 1. The graphene defogger reaches the saturated temperature faster than the Cr defogger; this is another advantage of the graphene defogger. The effective specific heat capacity of both defoggers is smaller than that of pure glass. This implies effective temperature increase can be achieved by coating additional graphene or Cr layers. The graphene layer forms a thermal interface to block heat dissipation more effectively than does the Cr layer. The input power vs. temperature was well-fitted by the theoretical curves (Figure 3b). The chromium defogger requires a higher power rate (27.7×10^{-4} W cm^{-2} °C^{-1}) than the graphene defogger (22.8×10^{-4} W cm^{-2} °C^{-1}).

Although we were able to obtain convective heat-transfer coefficients for the graphene/glass and Cr/glass defoggers and explain the general trend of better performance of graphene, with relatively low convective heat loss, the values of convective

Table 1. Power balance equation parameters for Cr/glass and graphene/glass systems.

	τ [s]	h [W m^{-2} °C^{-1}]	c* [J kg^{-1} °C^{-1}]	c [J kg^{-1} °C^{-1}]
Cr/glass	105	13.1	532	840
Graphene/glass	73	11.3	310	

Table 2. Convective heat - transfer coefficient of glass, graphene, and Cr thin film extracted by fitting the power loss model.

Material	h [W m^{-2} °C^{-1}]
Glass	11.1×10^{-4}
Graphene	12.4×10^{-4}
Cr thin film	17.1×10^{-4}

Table 3. The physisorption energies (meV) and distance from molecules to surface of graphene and chromium oxide cluster from generalized gradient approximation (GGA) calculations.

		O_2	N_2	H_2O
Graphene	E_{ad} [meV]	23	18	26
	d [Å]	3.42	3.59	3.08
Chromium	E_{ad} [meV]	143	148	290
	d [Å]	3.22	3.44	2.08

heat-transfer coefficient did not represent exclusively absolute values for the graphene and Cr thin-film, since they are combined with the glass substrate in the systems. We note that the temperature change $\Delta T = VI/(hA)$ is inversely proportional to the sample area. In order to determine the absolute values of convective heat-transfer coefficient for glass, graphene, and Cr, we used three different samples and extracted the absolute values by solving three linear equations (see the Supporting information, Figure S2 and Table S1). **Table 2** summarizes the convective heat-transfer coefficients of the three materials. The glass heat-transfer coefficient was found to be 11.1×10^{-4} W cm^{-2} °C^{-1}, similar to the previously reported values of 5–25 W m^{-2} °C^{-1} for free convection of air and 10–200 W m^{-2} °C^{-1} for forced convection of air.[26–28] The graphene heat-transfer coefficient was 12.4×10^{-4} W cm^{-2} °C^{-1}, similar to that of glass but much smaller (by 27%) than the 17.1×10^{-4} W cm^{-2} °C^{-1} of Cr thin film. This again explains why the graphene defogger shows better input power performance than does the Cr defogger in experiments.

The origin of the low convective heat-transfer coefficient of graphene, compared to the Cr thin film, could be due to the difference in: i) the surface roughness of the heating materials, and, ii) the thermal interfacial conductance between solid–gas adsorbates. To see the effect of surface roughness of heating materials, the graphene layer was over-coated with a Cr thin film. Since graphene follows the chromium surface roughness, in this case, the effect of the surface roughness can be ignored (see the supporting Information, Figure S3). A similar power dependence to Figure 3b was observed. This implies that the main origin of the difference is the thermal interfacial conductance between solid–gas adsorbates. The fact that the convective heat-transfer coefficient strongly relies on the material is related to molecular interactions at the surface, which mediate heat transfer from the solid to the air. It is known that ambient gas molecules, such as oxygen, nitrogen, and moisture, are physically adsorbed by van der Waals potential on the surface of solids. In general, convective heat transfer is directly influenced by the thermal interfacial conductance between solid–gas molecules, which is related to the thermal accommodation coefficient.[29] The thermal accommodation coefficient describes the exchange of heat energy from solid to gas molecules and is directly proportional to the gas adsorption energy. Here, we present density functional theory calculations for the adsorption energies of various ambient gases, including O_2, N_2, and H_2O (**Figure 5** and **Table 3**). Various physisorption sites were searched. Figure 5 shows a typical example of O_2-adsorbed graphene and chromium oxide clusters. O_2 adsorbs on the hexagonal site of graphene with a separation distance of 3.42 Å and an adsorption energy of 23 meV, which are comparable to previous works.[30] The real chromium surface may be oxidized under ambient conditions at atomic scale and therefore can be emulated by a simple cluster model. The O_2 adsorption energy on oxygen-saturated chromium cluster is 143 meV, much larger than for graphene. The results for other gases, N_2 and H_2O, (Table 3) show similar trends.

We now explain the heat-transfer mechanism in terms of competition between direct scattering and trapping–desorption

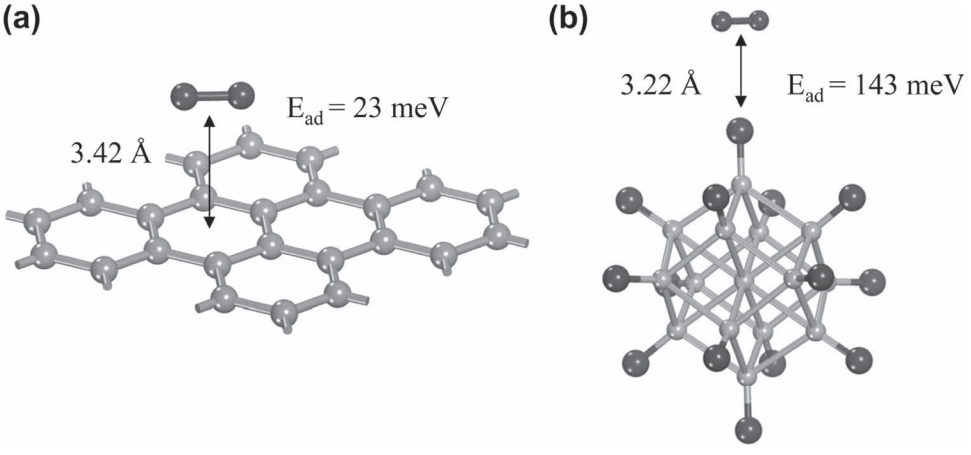

Figure 5. The geometry of physically adsorbed O_2 on the surface of: a) graphene and b) a chromium oxide cluster.

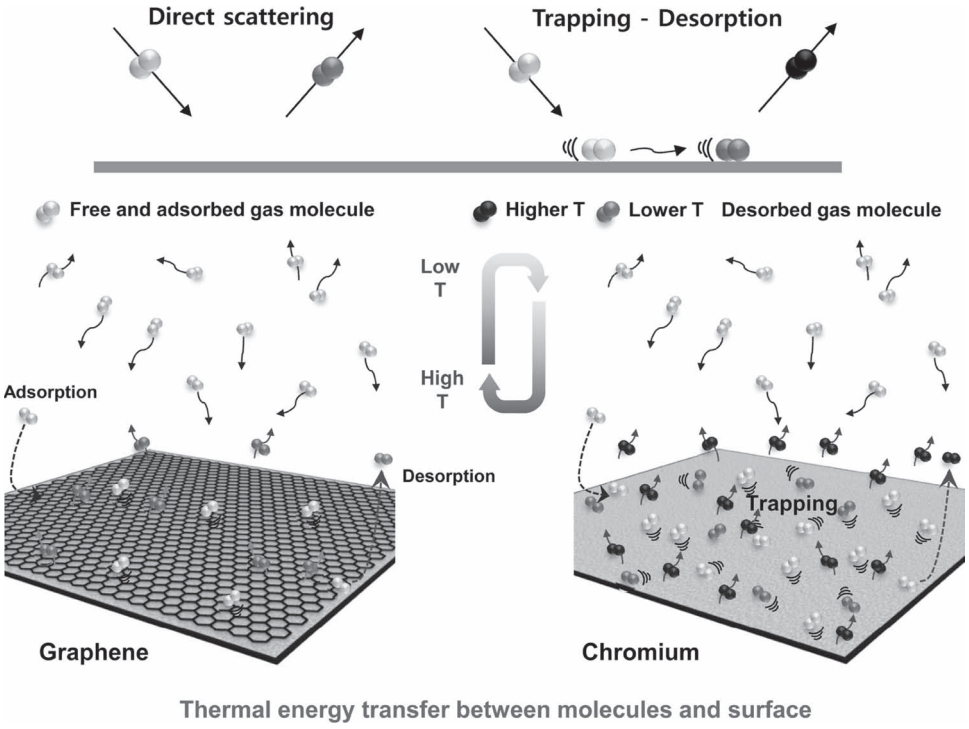

Figure 6. Schematics of direct scattering, trapping-desorption process of ambient gases and thermal energy transfer between molecules and electrode surface for graphene and Cr thin film defoggers.

of ambient gases,[31] as shown schematically in **Figure 6**. In the case of graphene, the adsorption energies of ambient gases, such as O_2, N_2, and H_2O, are relatively small and therefore the thermal accommodation coefficient is low. The ambient gases can be adsorbed but instantaneously desorb due to the comparable adsorption and thermal energies. Thermal interfacial conductance is poor in this case. On the other hand, the adsorption energies of ambient gases on the oxidized chromium surface are large, with an order of several hundreds meV. Therefore, they will be trapped for enough time to absorb heat from the solid surface before being released. The thermal interfacial conductance is large in this case. As a consequence, the convective heat-transfer coefficient of graphene is smaller than that of Cr thin film.

It is also intriguing to compare our graphene system with other nanocarbon-based systems. **Figure 7** shows temperature versus power density curves extracted from the literature. To compare our data to other types of nanocarbon-based systems, we further performed similar experiments with carbon nanotube (CNT) film, as done previously by other groups. While others studied heat performance in the low-power region, we obtained heat performance in the high-power region (Figure 7). Our high-power region of CNTs on glass was easily extrapolated from the low-power region data generated by others. This validates our approach in spite of the different measurement environments. The graphene/glass system revealed the best performance among all systems, including CNTs, RGOs, and metal thin films. We calculated heat performance and convective heat-transfer coefficients of the previously reported heating

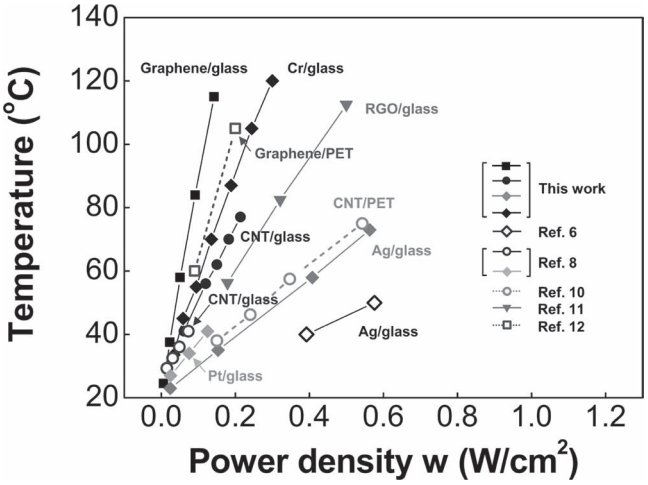

Figure 7. Electrical power density and saturated temperature of this work and other references.

systems; these are summarized in **Table 4**. Although the detailed experimental setup of the previous works was slightly different from our system, the overall convective heat-transfer coefficient of graphene is several times larger than those of CNTs or graphene oxide (GO)-based systems. It is also apparent to see the superior heat performance of the graphene system to conventional metal thin-films.

Table 4. Comparison of heat performance (H_p) and convective heat - transfer coefficients (h) extracted from other references.

Heating material	Substrate	H_p [10^{-4} m^2 °C W^{-1}]	h [W m^{-2} °C^{-1}]	Ref.	Notes
Graphene	Glass	660	8	This work	
	PET (close)*	409	12	[12]	
CNTs	Glass	212	24	This work	SWCNT film by a spray method
		208	25	[8]	SWCNT film by a dip-coating method
	PET (close)*	94	53	[10]	CNT yarn from vertical-aligned MWCNTs
RGO	Glass	163	32	[11]	Spin-coated GO/heat - treated
Cr	Glass	324	13	This work	E-beam evaporation
Ag		92	53	This work	Silver paste
		54	92	[6]	Silver paste
Pt		140	36	[8]	Sputtering

3. Conclusions

We fabricated a graphene/glass defogger and measured the dynamic responses of temperature as a function of input electrical power and voltage. The power-balance model, which includes the electrical power and the output temperature of the heating system, is proposed to explain the dynamic response of the temperature. By fitting the change of temperature with time to the proposed theoretical power balance model, the convective heat-transfer coefficients of graphene, glass, and chromium film were obtained. We found that the graphene has lower convective heat-transfer coefficient than Cr thin-film and, furthermore, the graphene-based heating system revealed much better heat performance in temperature vs power density than any other existing heating systems, including CNTs, RGOs, and conventional metal thin films. This opens a new possibility for numerous flexible and transparent heating systems, such as outdoor displays and vehicle front-window defrosters and defoggers.

4. Experimental Section

Synthesis of Monolayer Graphene: Monolayer graphene was synthesized on 70 μm thick Cu foil in atmosphere chemical vapor deposition (APCVD). Ar gas of 1000 standard cubic centimeters per minute (sccm) and H_2 gas of 200 sccm were fed into the chamber and temperature was elevated to 1050 °C for 40 min. The Cu foil was annealed at this temperature for 30 min before graphene synthesis. Graphene was synthesized at 1050 °C with a gas flow of H_2/CH_4 (10/5 sccm) for 5 min. The chamber was then allowed to cool down to room temperature with Ar gas supply.

Layer-by-Layer (LbL) Transfer of Graphene on to Glass Substrate: To transfer graphene to glass substrates, PMMA was coated on the prepared graphene/Cu foil, and then Cu was etched away by Cu etchant solution. After rinsing with distilled water to wash out etchant residues several times, PMMA-coated graphene (2 cm × 2 cm, 2.5 cm × 2.5 cm) was placed on glass substrate (4 cm × 4 cm, 3.5 cm × 3.5 cm) followed by a removal of PMMA with acetone. Three layers of graphene were obtained by repeated this process. For comparison, the chromium thin film (80 nm) was also prepared on glass substrate by an e-beam evaporator. Gold chloride ($AuCl_3$) powder was purchased from Sigma-Aldrich. $AuCl_3$ powder was dispersed in nitromethane at a concentration of 10 mM by sonication for 5 min. Once the graphene layer was transferred onto glass substrate, $AuCl_3$ solution was deposited on the graphene film by a spin coating method. Then the substrate was allowed to wait for 30 s to wet the surface of graphene, after which is spincoated at 1000 rpm for 1 min. This process was repeated several times to obtain several doped graphene layers.

Temperature Measurements: Cr (7 nm)/Au (70 nm) layer with an width of 1 mm was deposited at two edges of the prepared graphene/glass to apply the bias. Copper wires were connected to Cr/Au electrode by a silver paste. A DC current was applied on the defogger through a power supply (Agilent N5700). Profiles of temperature were measured with Omega K-type thermocouples which are physically contacted to the glass using a glue type and digital thermometer (Keithley 2700) at a given input voltage. The temperature measurements were performed at dry room, where the room temperature was controlled (±0.5 °C) during measurements.

Standard Calibration for the Temperature: We carried out standard calibration using a resistance-thermometer (RT) method by coating an Au thin film (3 mm × 1 mm × 20 nm) on the glass substrate to measure precisely the temperature. The 20 nm thick gold film was deposited on glass using e-beam evaporator, as shown in the Supporting Information, Figure S4a. This film was placed on the heating plate inside a closed cycle refrigerator (CCR). The resistance of the gold thin film was measured as a function of the CCR chamber temperature. The pressure of the CCR was about 2×10^{-6} torr and the temperature fluctuation of the sample, at the moment of the measurement, was less than 10 mK.

To characterize the resistance change of Au thin film, we adopted a four-point probe method (Figure S4a). Due to the low resistance of Au film, high current was necessary to apply to have a measurable voltage drop across the Au film. However, this could generate Joule heat that may modify the resistance of Au film. To minimize Joule heating effect on the Au film, minimum constant current was maintained (70 mA). This generated, for instance, 80 μV at room temperature. This Joule heating during short time measurement of 1 min increased the temperature of the substrate by 10^{-8} K, which is negligible. In addition, a small voltage range of μV may be misguided by the thermoelectric voltage, which is generated between two different metal wires connected to the Au film, here Au film and In wire. The possible contribution of the thermoelectric voltage was canceled out by changing the polarity of the applied current.[32] Furthermore, from the resistance change of Au film between temperature from 310 to 370 K, we extracted the temperature-coefficient of resistance (TCR) of Au, which is about $1.1–1.18 \times 10^{-3}$ K^{-1}. This value is comparable to the value in a previous report.[33] This indicates that the temperature calibration process in our work is reasonable and acceptable. For real calculations, the temperature of the glass was measured from thermocouple used in this study and RT method

(Figure S4a) by varying the temperature of the CCR chamber where the temperature of the sample was measured by the thermometer sensor installed on the heater.

The RT method overestimated the chamber temperature by 2.3 K, as shown in Figure S4, while the thermocouple underestimated the temperature by 1.4 K at 100 °C under atmospheric pressure. This value was much smaller than the difference of the saturation temperature between graphene and Cr heaters, as shown in Figure 3b. At the saturation, the temperature difference was roughly 20 °C. The main conclusion of the overall behavior of our heater was not altered by this temperature deviation.

Theoretical Calculations: Ab initio calculations were performed based on density functional theory (DFT) implemented by Dmol3 code with a double numerical plus polarization basic set.[34] For the exchange-correlation term, the generalized gradient approximation with Perdew-Burke-Enzerhof functional was employed.[35] The 4.8 Å cut-off orbital was used for all calculations. All models were optimized until the force was smaller than 0.002 Ha $Å^{-1}$. The adsorption energy was calculated by E_{ad} (substrate-molecule) = E_t (substrate-molecule) $-E_t$ (substrate) $-E_t$ (molecule), where E_t is the total energy of a given system. A periodic structure with $4 \times 4 \times 1$ *k*-point grid was used in the case of graphene. To emulate the chromium oxide surface, a chromium oxide cluster consisting of 15 chromium atoms and oxygen atoms covered on all chromium atoms so that no dangling bonds remained on the surface. This model is simple to construct and saves computing time but may provide slightly overestimated adsorption energies. In the case of physisorption, this difference is negligible; therefore, our calculation is limited only to the physisorption case.

Supporting Information

Supporting Information is available from the Wiley Online Library or from the author.

Acknowledgements

This work was supported by the Technology Innovation Program (10039486) funded by the Ministry of Knowledge Economy (MKE, Korea), the Star Faculty program (2010-0029653), and the World Class University (WCU) program (R31-2008-10029) of the National Research Foundation of Korea (NRF) and funded by the Ministry of Education, Science and Technology (MEST) of Korea.

Received: April 26, 2012
Published online: July 3, 2012

[1] C. G. Lee, X. Wei, J. W. Kysar, J. Hone, *Science* **2008**, *321*, 385–388.
[2] C. S. Ruiz-Vargas, H. L. Zhuang, P. Y. Huang, A. M. van der Zande, S. Garg, P. L. McEuen, D. A. Muller, R. G. Henning, J. W. Park, *Nano Lett.* **2011**, *11*, 2259–2263.
[3] R. R. Nair, P. Blake, A. N. Grigorenko, K. S. Novoselov, T. J. Booth, T. Stauber, N. M. R. Peres, A. K. Geim, *Science* **2008**, *320*, 1308–1308.
[4] A. K. Geim, K. S. Novoselov, *Nat. Mater.* **2007**, *6*, 183–191.
[5] K. S. Novoselov, A. K. Geim, S. V. Morozov, D. Jiang, Y. Zhang, S. V. Dubonos, I. V. Grigorieva, A. A Firsov, *Science* **2004**, *306*, 666–669.
[6] Y. H. Yoon, J. W. Song, D. J. Kim, J. D. Kim, J. K. Park, S. K. Oh, C. S. Han, *Adv. Mater.* **2007**, *19*, 4284–4287.
[7] Z. P. Wu, J. N. Wang, *Physica E* **2009**, *42*, 77–81.
[8] T. J. Kang, T. W. Kim, S. M. Seo, Y. J. Park, Y. H. Kim, *Carbon* **2011**, *49*, 1087–1093.
[9] D. J. Kim, H. C. Lee, J. Y. Woo, C. S. Han, *J. Phys. Chem. C* **2010**, *114*, 5817–5821.
[10] H. S. Jang, S. W. Jeon, S. H. Nahm, *Carbon* **2011**, *49*, 111–116.
[11] D. Sui, Y. Huang, L. Huang, J. J. Liang, Y. F. Ma, Y. S Chen, *Small* **2011**, *7*, 3186–3192.
[12] J. M. Kang, H. K. Kim, K. S. Kim, S. K. Lee, S. K. Bae, J. H. Ahn, Y. J. Kim, J. B. Choi, B. H. Hong, *Nano Lett.* **2011**, *11*, 5154–5158.
[13] G. H. Han, H. J. Shin, E. S. Kim, S. J. Chae, J. Y. Choi, Y. H. Lee, *Nano* **2011**, *6*, 59–65.
[14] F. Avilés, A. I. Oliva, J. A. Aznárez, *Appl. Surf. Sci.* **2003**, *206*, 336–344.
[15] A. I. Oliva, R. D. Maldonado, O. Ceh, J. E. Corona, *Surf. Rev. Lett.* **2005**, *12*, 289–298.
[16] M. Freitag, H. Y. Chiu, M. Steiner, V. Perebeinos, P. Avouris, *Nanotechnology* **2010**, *5*, 497–501.
[17] M. Freitag, M. Steiner, Y. Martin, V. Perebeinos, Z. H. Chen, J. C. Tsang, P. Avouris, *Nano Lett.* **2009**, *9*, 1883–1888.
[18] W. W. Cai, A. L. Moore, Y. W. Zhu, W. S. Li, S. S. Chen, L. Shi, R. S. Ruoff, *Nano Lett.* **2010**, *10*, 1645–1651.
[19] E. Pop, *Nano. Res.* **2010**, *3*, 147–169.
[20] Y. K. Koh, M. H. Bae, D. G. Cahill, E. Pop, *Nano Lett.* **2010**, *10*, 4363–4368.
[21] M. H. Bae, Z. Y. Ong, D. Estrada, E. Pop, *Nano Lett.* **2010**, *10*, 4787–4793.
[22] A. A. Balandin, *Nat. Mater.* **2011**, *10*, 569–581.
[23] F. Güneş, H. J. Shin, C. Biswas, G. H. Han, E. S. Kim, S. J. Chae, J. Y. Choi, Y. H. Lee, *ACS Nano* **2010**, *4*, 4595–4600.
[24] K. F. Mak, M. Y. Sfier, C. H. Lui, J. A. Misewich, T. F. Heinz, *Phys. Rev. Lett.* **2008**, *101*, 196405–196408.
[25] J. F. Papp, B. R. Lipin, *Chromium and Chromium Alloys: Kirk-Othmer Encyclopedia of Chemical Technology*; John Wiley & Sons, Inc, New York **2010.**
[26] I. Langmuir, *Phys. Rev.* **1912**, *34*, 401–422.
[27] I. Brody, F. Korosy, *J. Appl. Phys.* **1939**, *10*, 584–596.
[28] F. P. Incropera, D. P. DeWitt, *Fundamentals of Heat Transfer*; John Wiley & Sons, Inc, New York **1981.**
[29] M. Hu, S. Shenogin, P. Keblinski, N. Raravikar, *Appl. Phys. Lett.* **2007**, *90*, 231905–231907.
[30] P. Giannozzi, R. Car, G. Scoles, *J. Chem. Phys.* **2003**, *118*, 1003–1006.
[31] G. Fan, J. R. Manson, *Phys. Rev. B* **2009**, *79*, 045424–045437.
[32] J. F. Keithley, *Low Level Measurements Handbook: Precision DC Current, Voltage, and Resistance Measurements, 6th Edition*, Keithley Instruments, Inc, Cleveland, OH **2004**, 3.16–3.22.
[33] W. Ma, X. Zhang, K. Takahashi, *J. Phys. D: Appl. Phys.* **2010**, *43*, 465301–465308.
[34] B. Delley, *Phys. Rev. B* **2002**, *66*, 155125–155133.
[35] J. P. Perdew, K. Burke, M. Ernzerhof, *Phys. Rev. Lett.* **1996**, *77*, 3865–3868.